

A Study of Wavelets for the Solution of Electromagnetic Integral Equations

Robert L. Wagner, *Student Member*, and Weng Cho Chew, *Fellow, IEEE*

Abstract—The use of wavelet basis functions for the efficient solution of electromagnetic integral equations is studied. It has previously been demonstrated that the use of wavelets for expansion and testing functions produces a sparse moment-method matrix. Here, this effect is examined and analyzed in terms of the radiation/receiving characteristics of the wavelet basis functions. The limitations of wavelets as an efficient solution technique are discussed, and a comparison is made to other fast algorithms.

I. INTRODUCTION

RECENTLY, the use of wavelets and wavelet-like basis functions for the efficient solution of electromagnetic integral equations has received considerable attention [1]–[4]. Mathematicians originally applied wavelets to the solution of integral operator equations having essentially smooth, non-oscillatory kernels (such as those encountered in electrostatics) [5]–[6]. Use of wavelets as a solution basis produces a sparse interaction matrix which may be solved rapidly. For such problems, wavelets can be used to obtain a solution in $O(N \log N)$ operations, where N is the number of unknowns in the discretized integral equation [5]–[6]. This is in contrast with a cost of $O(N^3)$ for a dense matrix inversion or $O(N^2)$ per dense matrix-vector multiply in an iterative solution such as conjugate-gradient. Clearly, wavelets are a powerful technique for solving such equations efficiently. In the electrodynamic case, the integral equation has an oscillatory kernel. While in this case wavelets do not produce as dramatic a saving as for smooth kernels, they still produce significant sparsity in the operator matrix. In this paper, we focus attention on the application of wavelets to efficiently solve for the electromagnetic scattering from two-dimensional conducting cylinders using a combined field integral equation (CFIE)/method of moments (MoM) approach. First, we briefly review the CFIE/MoM problem formulation using a typical pulse basis and discuss the properties of the wavelet basis functions. We then discuss the use of wavelets for solving the MoM matrix equation and analyze their effectiveness in terms of the radiation/receiving characteristics of the wavelet basis functions. Results are presented, the limitations of wavelets as

an efficient solution technique are discussed, and a comparison is made to other fast algorithms.

II. PROBLEM FORMULATION

The problem considered here is that of computing the scattering of a TM (E_z) polarized electromagnetic wave from a two-dimensional conducting cylinder with boundary contour C . The incident wave E_z^{inc} excites a surface current J_z on the surface of the cylinder which produces a scattered field E_z^{scat} . Enforcing the boundary condition that the total field E_z must vanish on C yields the electric field integral equation (EFIE)

$$E_z^{\text{inc}}(\mathbf{r}) = -E_z^{\text{scat}}(\mathbf{r}) = -i\omega\mu_0 \oint_C dl' J_z(\mathbf{r}') g_0(\mathbf{r}, \mathbf{r}'), \quad \mathbf{r} \in C \quad (1)$$

where g_0 is the two-dimensional Green's function [$g_0(\mathbf{r}, \mathbf{r}') = (i/4)H_0^{(1)}(k_0|\mathbf{r} - \mathbf{r}'|)$], and k_0 is the wavenumber. A time dependence of $e^{-i\omega t}$ is assumed.

Because the EFIE is ill conditioned at the resonant frequencies of the cylinder C , we make use of the CFIE which is free of resonance problems. The CFIE may be derived by applying the differential operator $P(\mathbf{r}) = 1 + \alpha \hat{n} \cdot \nabla$ to both sides of (1), yielding

$$E_z^{\text{inc}}(\mathbf{r}) + \alpha \frac{\partial E_z^{\text{inc}}(\mathbf{r})}{\partial n} = -i\omega\mu_0 \oint_C dl' J_z(\mathbf{r}') \left[g_0(\mathbf{r}, \mathbf{r}') + \alpha \frac{\partial g_0(\mathbf{r}, \mathbf{r}')}{\partial n} \right], \quad \mathbf{r} \in C. \quad (2)$$

The constant α is the CFIE combination parameter.

Discretizing (2) using a pulse basis for J_z and point matching yields the MoM matrix formulation

$$\mathbf{e} = \mathbf{Z} \cdot \mathbf{j} \quad (3)$$

where \mathbf{Z} is a full nonsymmetric matrix with elements which can be approximated as

$$Z_{ij} = \frac{\omega\mu_0}{4} \begin{cases} \Delta_j \left[1 + i \frac{2}{\pi} \ln \left(\frac{e^\gamma k_0 \Delta_j}{4e} \right) \right] - 2i\alpha, & i = j \\ \Delta_j \left[H_0^{(1)}(k_0|\mathbf{r}_i - \mathbf{r}_j|) \right] \\ -\alpha k_0 \left(\hat{n}_i \cdot \frac{\mathbf{r}_i - \mathbf{r}_j}{|\mathbf{r}_i - \mathbf{r}_j|} \right) H_1^{(1)}(k_0|\mathbf{r}_i - \mathbf{r}_j|) \end{cases} \quad (4)$$

Manuscript received April 1, 1994; revised April 10, 1995. This work was supported in part by the Office of Naval Research under grant N00014-89-J-1296, by the Army Research Office under contracts DAAL03-91-G-0339 and DAAH04-93-G-0430, by NASA under contract NASA-NAG-2-871, and by the National Science Foundation under grant NSF-ECS-92-24466.

The authors are with the Electromagnetics Laboratory, Department of Electrical and Computer Engineering, University of Illinois, Urbana, IL 61801 USA.

IEEE Log Number 9412903.

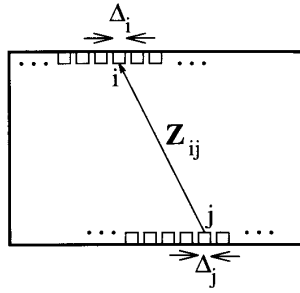


Fig. 1. Physical interpretation of the pulse basis MoM matrix Z . The matrix element Z_{ij} is the field radiated by unit amplitude current pulse j sampled at the midpoint of receiving pulse i .

where $\gamma = 0.5772$ is Euler's constant, and Δ_i , \mathbf{r}_i , and $\hat{\mathbf{n}}_i$ are the width, center position, and outgoing normal to C , respectively, for the i th pulse. Typically, the pulse width is chosen to be $\Delta_i \approx \lambda_0/10$, where λ_0 is the free-space wavelength. This discretization density is used throughout this paper.

The elements of Z are physically meaningful; Z_{ij} represents the field radiated by a unit amplitude current pulse j sampled at the midpoint of the receiving pulse i . This is illustrated in Fig. 1. Because the CFIE is used, the sampled field is a linear combination of the z -directed electric field and the component of the transverse magnetic field tangent to the boundary C . Since square pulses are relatively good radiators, Z is a full matrix. An example of the dense, oscillatory nature of Z is shown in Fig. 2.

Because Z is a full matrix, solution of (3) is expensive. For a problem with N unknowns, direct solution of (3) has a computational cost of $O(N^3)$. For an iterative solution, each iteration will have a cost of $O(N^2)$ which is the cost of a dense matrix-vector multiply. It is this high solution cost which motivates the study of wavelets as a means for obtaining an efficient solution.

III. THE WAVELET BASIS

Here we give a brief description of the wavelet basis functions which will be used in this work. We begin by noting that we are already working with a discretized problem (3). Thus, we desire a set of N orthonormal vectors which form a basis for the N -dimensional vector space \mathbf{R}^N . (Strictly speaking, it is not necessary that the vectors be orthonormal. Use of an orthonormal basis set simplifies, however, the change of basis calculations.) Note also that we are working with a one-dimensional discretization; the original pulses are arranged sequentially along the boundary curve C of the cylindrical scatterer.

The basis vectors used here have two principal properties. First, they have support on different length scales in space. That is, some of the basis vectors have very compact support (localized in space), while others have broader support (more spread out in space). All spatial resolutions are included in the basis set, up to the vectors with the broadest support, which covers the whole discretization region. Thus, the basis vectors

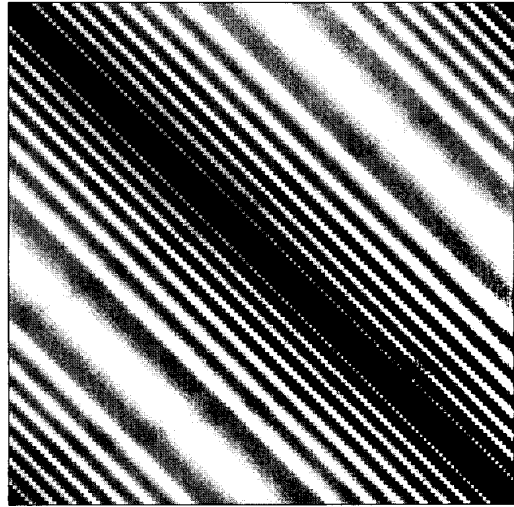


Fig. 2. An example of the dense, oscillatory nature of the pulse basis MoM matrix Z . This is a grayscale image of the magnitude of the real part of Z for a circular cylinder with circumference $12.8 \lambda_0$. The cylinder is discretized into 128 pulses of width $\lambda_0/10$.

form a "multiresolution" representation of the surface current on the boundary C . Second, almost all of the basis vectors have a certain number p of vanishing moments, where p is a parameter chosen by the user. By p vanishing moments, it is meant that for a basis vector \mathbf{b} with elements $\{b_i\}_{i=1, \dots, N}$, the following holds

$$\sum_{i=1}^N b_i \cdot i^j = 0, \quad j = 0, 1, \dots, p-1. \quad (5)$$

To have a complete set of basis vectors, there must be a small number of vectors which do not have the above property (to represent very smooth elements of \mathbf{R}^N). These few smooth basis vectors correspond to the "scaling functions" ϕ of wavelet theory [7].

Having outlined the general properties of wavelet basis vectors, we turn now to the specific bases to be used here. For this work we make use of perhaps the best-known wavelets, discovered by Daubechies [8]. An example is shown in Fig. 3. Fig. 3(a), a grayscale image of the matrix U which has the wavelet basis vectors as its rows, shows the organization of all the vectors making up the basis. The different bands in the image correspond to the different resolution scales in the basis. Sample basis vectors (rows of U) are plotted in Fig. 3(b). The basis vectors in this example form a complete orthonormal basis for \mathbf{R}^N with $N = 128$ points and $p = 8$ vanishing moments. These basis vectors are true wavelets as can be seen in Fig. 3(b); they are (almost) all translations and dilations of a single "mother wavelet." Translations of the finest resolution wavelet comprise one half of the basis set; translations of the next finest resolution wavelet make up one quarter of the set, and so on down the hierarchy. We used the computer programs in [9] to generate and manipulate these basis vectors.

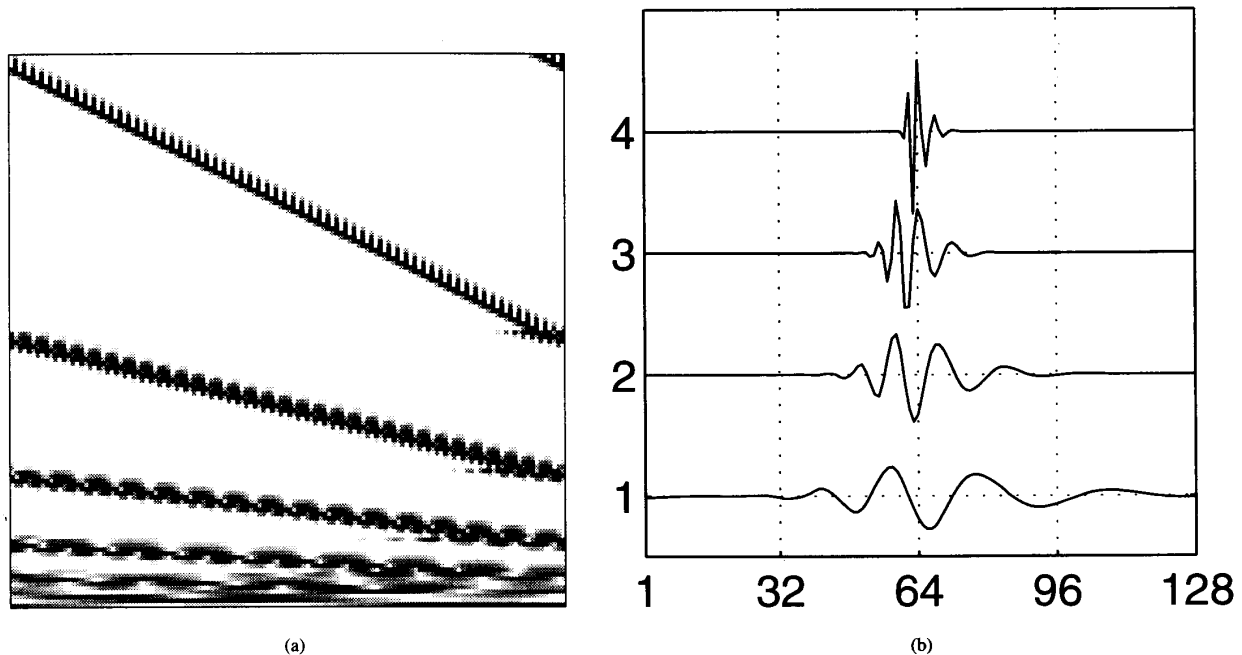


Fig. 3. (a) Magnitude of the basis vector matrix U for the Daubechies wavelets with $N = 128$ discretization points and $p = 8$ vanishing moments. Each row is one basis vector. (b) Sample basis vectors: rows 35, 82, 106, and 118 of U .

Our previous work [4] made use of the wavelet-like bases of Alpert *et al.* [6]. As for the Daubechies wavelets, this set forms a complete orthonormal basis for \mathcal{R}^N and has the same multiresolution and vanishing moment properties. This basis differs from a classical wavelet basis in that basis vectors at different resolutions are not all dilations and translations of the same “mother wavelet.” In fact, at each resolution level there is a set of p overlapping (but still orthonormal) basis vectors which are all translated to cover the discretized space. These basis vectors are constructed using orthogonal polynomials (Gram–Schmidt orthogonalization). For electromagnetics problems, we have observed almost identical results using the Daubechies wavelets and the wavelet-like bases of [6] with the same number of vanishing moments p . Here we choose to use the Daubechies wavelets because they may be familiar to a greater number of readers.

Note that the wavelet basis vectors can be constructed for different values of p and N . For convenience, N is usually chosen to be a power of two; the choice of p will be discussed in Section V. Finally, we note that the transformation of a vector of length N to wavelet coordinates can be computed in $O(N)$ operations using the fast wavelet transform [9]. Correspondingly, an $N \times N$ matrix can be transformed in $O(N^2)$ operations.

IV. WAVELET TRANSFORM OF THE MOM IMPEDANCE MATRIX

Having described the wavelet basis vectors in Section III, we now examine their effect on the MoM impedance matrix Z of Section II. Let U be an $N \times N$ matrix with the new basis vectors as its rows. Because the vectors form an orthonormal basis for \mathcal{R}^N , U is an orthogonal matrix satisfying $U^T = U^{-1}$.

To switch to the new basis set, a similarity transformation is performed on (3), to obtain

$$Ue = UZU^T \cdot Uj \quad (6)$$

or

$$e' = Z' \cdot j' \quad (7)$$

where $e' = Ue$, $j' = Uj$, and the transformed impedance matrix is $Z' = UZU^T$.

After transformation to a wavelet basis, the new impedance matrix Z' is found to be approximately sparse. That is, many of its matrix elements are negligibly small. To take advantage of this, elements of Z' which are smaller than an element threshold τ are discarded, and the remaining elements of Z' are stored in sparse matrix form. (We use the “row-indexed sparse storage mode” described in [9]. This allows matrix-vector multiplications to be carried out in a time proportional to the number of non-zero elements in the sparse matrix, speeding the iterative solution of the transformed matrix equation.) As in [4], [6], we choose the threshold to be

$$\tau = \frac{\delta}{N} \|Z\|_{\infty} \quad (8)$$

where δ is a constant, N is the dimension of Z , and $\|Z\|_{\infty}$ is the infinity or row-sum norm of Z , $\|Z\|_{\infty} = \max_i \sum_{j=1}^N |Z_{ij}|$.

Examples of a transformed impedance matrix Z' are shown in Figs. 4 and 5. The Daubechies wavelets with $p = 8$ vanishing moments are used. Fig. 4 shows the new impedance matrix Z' for a circular cylinder of circumference $12.8 \lambda_0$, discretized with 128 pulses of width $\lambda_0/10$ (compare with

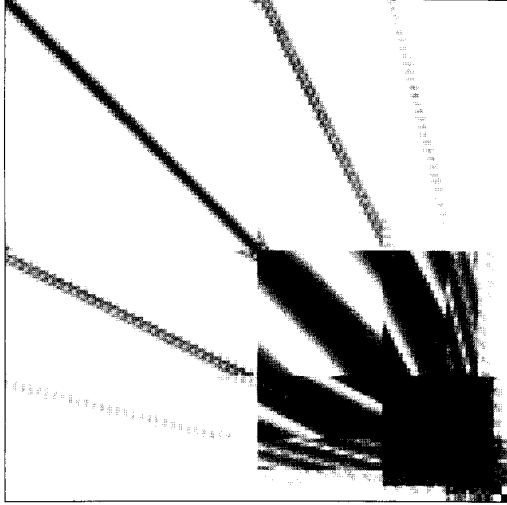


Fig. 4. Wavelet-domain impedance matrix Z' for a circular cylinder of circumference $12.8 \lambda_0$, discretized with 128 pulses of width $\lambda_0/10$ (compare with Fig. 2). The matrix is transformed using the Daubechies wavelets with $p = 8$ vanishing moments. This is a grayscale image of the magnitude (on a log scale) of the elements of Z' , showing only elements with magnitude greater than 10^{-4} of the maximum element. The largest elements are in black.

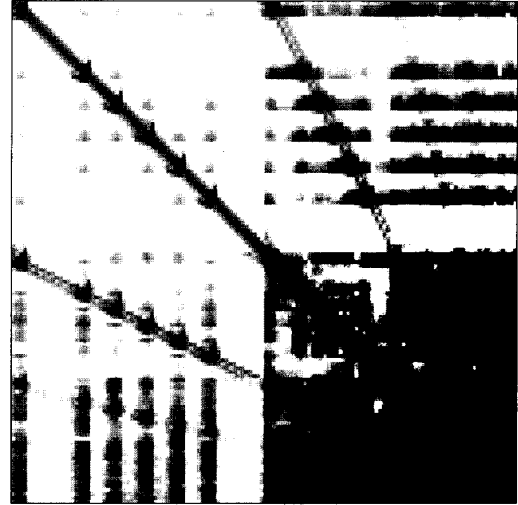


Fig. 5. Wavelet-domain impedance matrix Z' for the L-shaped scatterer of Fig. 6 with side length $l = 3.2\lambda_0$. The scatterer is discretized with 128 pulses of width $\lambda_0/10$. The matrix is transformed using the Daubechies wavelets with $p = 8$ vanishing moments. This is a grayscale image of the magnitude (on a log scale) of the elements of Z' showing only elements with magnitude greater than 10^{-4} of the maximum element. The largest elements are in black.

Fig. 2). This is a grayscale image of the magnitude (on a log scale) of the elements of Z' showing only elements with magnitude greater than 10^{-4} of the maximum element. The largest elements are in black. Fig. 5 is a similar image of the matrix for an L-shaped scatterer as shown in Fig. 6. Again, the scatterer is discretized with 128 pulses of width $\lambda_0/10$.

From Figs. 4 and 5, we can make some qualitative observations about the wavelet-domain impedance matrix Z' . Note that the elements of Z' represent the interactions between wavelet sources and receivers rather than between the pulse current sources and point receivers of the original matrix Z (as illustrated in Fig. 1). The multi-scale nature of the basis is easily seen. In both figures, the upper left quadrant represents the interactions between basis functions with the smallest spatial support (finest resolution level). This portion of the matrix is very sparse and diagonally dominant indicating that these basis functions do not interact strongly with one another when they are spatially separated. In Fig. 5, there are extra interactions in this portion of the matrix associated with the strong scattering from the corners of the L-shaped object. Moving along the diagonal toward the lower right corner of the matrix, there are similar (smaller) blocks which represent interactions between basis functions at the same resolution level. The interactions become stronger as the spatial support of the basis functions broadens. In the off-diagonal blocks, there are "fingers" which represent the interaction between basis functions on different resolution levels. These interactions are strongest when the two basis functions overlap in space. Again, there are extra interactions for the L-shaped scatterer because of the corners. The blocks with the greatest sparsity always involve interactions with the finest resolution basis functions.

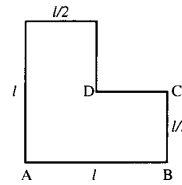


Fig. 6. Geometry of the L-shaped scatterer whose wavelet-domain impedance matrix is shown in Fig. 5.

V. RADIATION CHARACTERISTICS OF WAVELETS

A deeper understanding of the structure of the wavelet-domain impedance matrix Z' can be gained by considering the radiation/receiving characteristics of the wavelet basis functions. If a surface current J_z exists on a two-dimensional boundary C , the radiated electric field is (as in (1))

$$E_z(\mathbf{r}) = i\omega\mu_0 \int_C dl' J_z(\mathbf{r}') g_0(\mathbf{r}, \mathbf{r}') \quad (9)$$

where g_0 is the two-dimensional Green's function [$g_0(\mathbf{r}, \mathbf{r}') = (i/4)H_0^{(1)}(k_0|\mathbf{r} - \mathbf{r}'|)$]. Using the asymptotic form for the Hankel function

$$H_0^{(1)}(x) \sim \sqrt{\frac{2}{\pi x}} e^{i(x - \pi/4)}, \quad x \rightarrow \infty \quad (10)$$

and the far-field approximations

$$\frac{1}{\sqrt{|\mathbf{r} - \mathbf{r}'|}} \sim \frac{1}{\sqrt{|\mathbf{r}|}} \quad |\mathbf{r}| \gg |\mathbf{r}'|, \quad (11a)$$

$$e^{ik_0|\mathbf{r} - \mathbf{r}'|} \sim e^{ik_0(r - \hat{r} \cdot \mathbf{r}')}, \quad |\mathbf{r}| \gg |\mathbf{r}'| \quad (11b)$$

one obtains the far-field radiation expression

$$E_z(\mathbf{r}) = \frac{e^{ik_0 r}}{\sqrt{r}} \cdot -\frac{\omega\mu_0}{4} \left(\frac{2}{i\pi k_0} \right)^{1/2} \int_C dl' J_z(\mathbf{r}') e^{-ik_0 \hat{r} \cdot \mathbf{r}'} \quad (12)$$

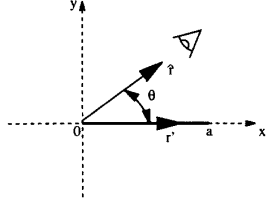


Fig. 7. Geometry for computing the far-field radiation from a straight current strip. The current lies on the x -axis from $x = 0$ to $x = a$. The observation direction \hat{r} makes an angle θ with the x -axis.

where $r = |\mathbf{r}|$ and $\hat{r} = \mathbf{r}/r$. Specializing one step further, suppose the boundary C is a straight line segment as shown in Fig. 7. Then $\hat{r} \cdot \mathbf{r}' = x' \cos \theta$ and the far-field radiation is

$$E_z(\mathbf{r}) = \frac{e^{ik_0 r}}{\sqrt{r}} \cdot -\frac{\omega\mu_0}{4} \left(\frac{2}{i\pi k_0} \right)^{1/2} \cdot \int_0^a dx' J_z(x') e^{-i(k_0 \cos \theta)x'}. \quad (13)$$

Using the Fourier transform pair

$$\tilde{J}_z(k_x) = \int_0^a dx e^{-ik_x x} J_z(x) \quad (14a)$$

$$J_z(x) = \frac{1}{2\pi} \int_{-\infty}^{\infty} dk_x e^{ik_x x} \tilde{J}_z(k_x) \quad (14b)$$

(13) becomes

$$E_z(\mathbf{r}) = \frac{e^{ik_0 r}}{\sqrt{r}} \cdot -\frac{\omega\mu_0}{4} \left(\frac{2}{i\pi k_0} \right)^{1/2} \tilde{J}_z(k_0 \cos \theta). \quad (15)$$

Thus, the far-field radiation of the strip is proportional to the one-dimensional Fourier transform of the current evaluated at the wavenumber $(k_0 \cos \theta)$. Of particular importance is that if the current has only high spatial frequency content (above k_0), it will produce no far-field radiation; the fields will be evanescent and decay rapidly away from the location of the current.

Further insight can be gained from considering the spectral representation of the Hankel function [10]

$$H_0^{(1)}(k_0 |\mathbf{r} - \mathbf{r}'|) = \frac{1}{\pi} \int_{-\infty}^{\infty} dk_x \frac{e^{ik_x(x-x') + ik_y|y-y'|}}{k_y} \quad (16)$$

where $k_y = \sqrt{k_0^2 - k_x^2}$ with $\Im m[k_y] > 0$ to satisfy the radiation condition at infinity. Inserting this expression into (9) and assuming the strip geometry of Fig. 7 yields the expression

$$E_z(\mathbf{r}) = -\frac{\omega\mu_0}{4\pi} \int_0^a dx' J_z(x') \int_{-\infty}^{\infty} dk_x \frac{e^{ik_x(x-x') + ik_y|y|}}{k_y}. \quad (17)$$

Interchanging the order of integration

$$\begin{aligned} E_z(\mathbf{r}) &= -\frac{\omega\mu_0}{4\pi} \int_{-\infty}^{\infty} dk_x \frac{e^{ik_x x + ik_y|y|}}{k_y} \int_0^a dx' J_z(x') e^{-ik_x x'} \\ &= -\frac{\omega\mu_0}{4\pi} \int_{-\infty}^{\infty} dk_x \frac{e^{ik_x x + ik_y|y|}}{k_y} \tilde{J}_z(k_x). \end{aligned} \quad (18)$$

From (18), it is seen that spectral components of the current $\tilde{J}_z(k_x)$ with $k_x > k_0$ produce a radiated field which decays exponentially in the $\pm y$ direction with decay rate $e^{-\sqrt{k_x^2 - k_0^2}|y|}$.

To relate this result to (15), the above integral may be approximated using the method of stationary phase [10]. For large absolute values of x and y , the integrand in (18) is rapidly oscillating. The main contribution to the integral comes from the value of k_x where the integrand has the least rapid oscillation. This point, called the stationary-phase point, is where

$$\frac{d}{dk_x} [k_x x + k_y |y|] = 0. \quad (19)$$

Using the relationship $k_y = \sqrt{k_0^2 - k_x^2}$, the stationary-phase point is found to be

$$k_{xs} = k_0 \frac{x}{\sqrt{x^2 + y^2}} = k_0 \cos \theta \quad (20)$$

where $\theta = \cos^{-1}(x/\sqrt{x^2 + y^2})$ is the observation angle measured from the x -axis. Now, using the stationary phase idea, the integral in (18) may be approximated as

$$\begin{aligned} E_z(\mathbf{r}) &\sim -\frac{\omega\mu_0}{4\pi} \tilde{J}_z(k_{xs}) \int_{-\infty}^{\infty} dk_x \frac{e^{ik_x x + ik_y|y|}}{k_y} \\ &= -\frac{\omega\mu_0}{4} \tilde{J}_z(k_0 \cos \theta) H_0^{(1)}(k_0 r), \quad r \rightarrow \infty. \end{aligned} \quad (21)$$

Substituting the asymptotic expression (10) for the Hankel function above, this is seen to be identical to (15).

Since the current on the strip has finite spatial support, it cannot have zero spectral content over the entire "visible region" $k_x \leq k_0$; it must have some radiating spectral components. The current may still be approximately localized in spatial frequency, however, with the radiating components being orders of magnitude smaller than the nonradiating components. This is possible with basis functions such as the Daubechies wavelets which are strictly localized in space and approximately localized in spatial frequency. Some of the high-frequency wavelets produce fields which are highly localized with very small radiating components.

This effect can be seen clearly in Figs. 8 and 9. Fig. 8 shows the magnitude of the fields radiated by the wavelet currents of Fig. 3(b). The currents are assumed to be located on the surface of a circular cylinder of circumference $12.8 \lambda_0$. The radiated field is evaluated at 128 observation points on the surface of the same cylinder. The magnitudes of the Fourier transforms of the currents are shown in Fig. 9. It can be seen that the most spatially compact currents (labeled 3 and 4 in the figures) have little spectral content in the "visible region" $k_x \leq k_0$. Thus, we expect these currents to produce highly localized fields, which is the case. The fields due to these currents are almost entirely spatially localized to the support of the currents. The remaining two currents (labeled 1 and 2) have broader spatial support and lower spatial frequency content with spectra extending into the "visible range." Thus we expect them to radiate over the whole boundary, and this is seen to be case.

This explains much of the structure of the wavelet-domain impedance matrixes shown in Figs. 4 and 5. The weak interactions associated with the first two (finest resolution) levels of basis functions are due to the local nature of the

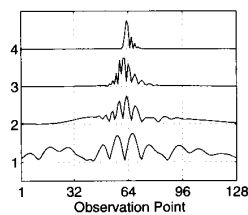


Fig. 8. Magnitudes of the fields radiated by the wavelet currents of Fig. 3(b). The currents are assumed to be located on the surface of a circular cylinder of circumference $12.8 \lambda_0$. The radiated field is evaluated at 128 observation points on the surface of the same cylinder.

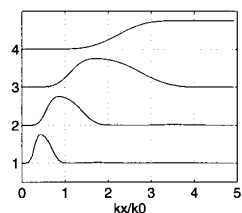


Fig. 9. Magnitudes of the Fourier transforms of the wavelet currents of Fig. 3(b) assuming a discretization density of 10 points per wavelength. Currents 3 and 4 have little spectral content in the “visible region” $k_x \leq k_0$.

radiation/receiving properties of these functions. The remaining basis functions have broader support, are better radiators/receivers, and hence have stronger interactions with one another. Note that the analysis leading to (15) is specialized for the case of currents on a straight strip. As seen in this example, however, the concept remains approximately true for currents on curved boundaries as long as the bending is not too great. For the case of the L-shaped scatterer, there are sharp corners which alter the radiation properties of the wavelet currents producing the extra interactions between fine-scale wavelets seen in Fig. 5.

Based on these observations, we expect that for asymptotically large surfaces which are essentially smooth, with only a few sharp bends or corners, around 75% of the wavelet basis functions (the 50% at the finest resolution and 25% at the next finest resolution) should have very limited interactions. The strong interactions between the remaining 25% of the basis functions should account for most of the important elements of Z' , resulting in a wavelet-domain matrix with a sparsity of approximately $0.25 \times 0.25 = 0.0625$, or 6.25% nonzero elements. Note that this figure is tied to the choice of discretization density (10 points per wavelength here). A finer discretization would result in more basis functions producing only evanescent fields. This would result in greater sparsity but at the cost of more unknowns for a given problem. Also, the sparsity depends on the specific choice of wavelet basis, as this determines the spectral content and hence the radiation properties of the different basis functions.

In particular, the Daubechies wavelets are constructed with p vanishing moments, where p is an adjustable parameter. Sample basis vectors and their Fourier transforms are shown in Figs. 3 and 9 for the case $p = 8$ and in Figs. 10 and 11 for the cases $p = 2$ and $p = 10$. In all these cases, the scaling of the spatial frequency axis assumes a discretization density of 10

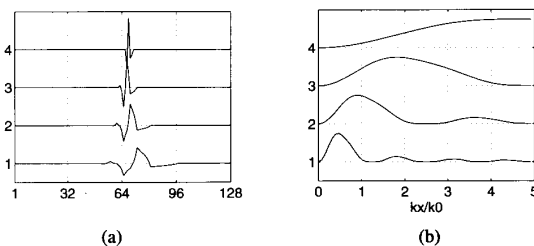


Fig. 10. (a) Sample basis vectors for the Daubechies wavelets with $N = 128$ discretization points and $p = 2$ vanishing moments. (b) Magnitudes of the Fourier transforms of the wavelets in (a) assuming a discretization density of 10 points per wavelength.

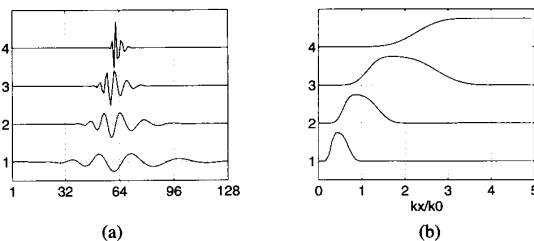


Fig. 11. (a) Sample basis vectors for the Daubechies wavelets with $N = 128$ discretization points and $p = 10$ vanishing moments. (b) Magnitudes of the Fourier transforms of the wavelets in (a) assuming a discretization density of 10 points per wavelength.

points per wavelength. As can be seen in the figures, increasing p produces smoother, broader basis functions with sharper spectral cutoffs. When $p = 2$, the spectral transitions are gradual, and the high frequency basis functions have spectra which leak over into the “visible region” allowing these basis functions to radiate. Thus, the use of this basis set will not produce good matrix sparsity. Comparing the cases $p = 8$ and $p = 10$, it can be seen that there is not a large difference between the spectral transitions of these two basis sets; they both have reasonably sharp cutoffs and will produce matrixes with similar levels of sparsity. The wavelets with $p = 10$ offer only a slight improvement over those with $p = 8$. In addition, there are disadvantages to making p too large. First, the cost of the fast wavelet transform is proportional to p . This is an important practical consideration, as the matrix transformation time can be significant. With $p = 8$, we found the matrix transformation time to be close to the matrix fill time. Second, when p becomes large, the basis functions have broader spatial support and hence are more susceptible to the effects of bending due to the scatterer geometry. This could adversely affect the matrix sparsity. Based on these considerations, we have used $p = 8$ vanishing moments to obtain the results of this paper.

VI. RESULTS (MATRIX SPARSITY)

From our computer experiments, we have found that good solution accuracy can often be obtained by retaining only around 10% of the elements of the transformed matrix Z' . As a measure of solution accuracy, we use the relative residual error $\|Z \cdot \mathbf{j}_{\text{comp}} - \mathbf{e}\|/\|\mathbf{e}\|$, where \mathbf{j}_{comp} is the solution computed using the thresholded sparse matrix Z' , and the

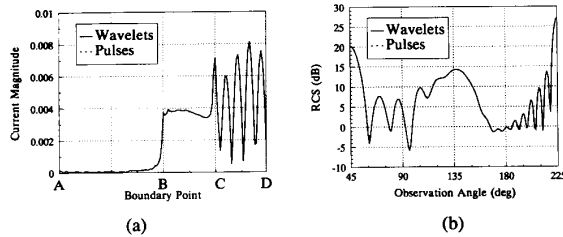


Fig. 12. (a) Induced surface current J_z and (b) Bistatic RCS for the L-shaped cylinder of Fig. 6. The scatterer has edge length $l = 6.4\lambda_0$ and is discretized with $N = 256$ pulses of width $\lambda_0/10$. The excitation is an E_z polarized plane wave incident from 45 degrees into the concave corner of the L.

norm is the standard Euclidean norm of a vector. To achieve a relative residual error of $\sim 1\%$ typically required a choice of $\delta \sim 0.1-0.2$ for computing the element threshold τ in (8). An example of a scattering calculation using wavelets is shown in Fig. 12. Here the scatterer is the L-shaped cylinder of Fig. 6 with edge length $l = 6.4\lambda_0$ originally discretized with $N = 256$ pulses of width $\lambda_0/10$. The Daubechies wavelets with $p = 8$ vanishing moments are used. The threshold parameter is $\delta = 0.1$, and the computed solution has a relative residual error of 0.99%. The transformed and thresholded matrix had a sparsity of 19.75% nonzero elements. As can be seen, the results for both surface current and radar cross section (RCS) are in good agreement with the solution obtained using the original dense matrix.

To study the relationship between problem size and matrix sparsity for a fixed solution accuracy, we computed the scattering from circular cylinders of increasing size, adjusting the element threshold to maintain a solution error of $(1 \pm 0.01)\%$. The discretization density was kept fixed at 10 points per wavelength. The results are shown in Fig. 13. Increasing the problem size from $N = 256$ unknowns (a circle of diameter $25.6\lambda_0$) to $N = 8192$ unknowns (a circle of diameter $819.2\lambda_0$), the sparsity of Z' varied from a high of 10.0% non-zero elements for the 256 unknown problem to a low of 6.18% for the 8192 unknown problem. As can be seen in the figure, the sparsity changes rather quickly for smaller problems and flattens out for large N . These results suggest that for a large smooth surface, the sparsity is only a very weak function of problem size.

A similar experiment was carried out for the L-shaped scatterer. The problem size was increased while the discretization density was kept fixed at 10 points per wavelength, and a solution accuracy of $(1 \pm 0.02)\%$ was maintained. Increasing the problem size from $N = 256$ to $N = 4096$ unknowns, the sparsity varied from 19.75% non-zero elements for the 256 unknown problem to 8.15% for the 4096 unknown problem. This relatively large change in sparsity is due to the diminishing importance of the corners relative to the smooth parts of the surface as the problem scales. For larger problems, we would expect the sparsity to eventually approach that of the circular cylinder. (The calculations for the L-shaped scatterer are not carried out for larger N because of computational limitations. For the circular cylinder, the circulant structure of the pulse-basis MoM matrix allows the solution of larger problems.)

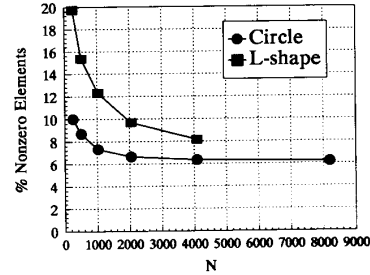


Fig. 13. Matrix sparsity as a function of problem size for the circular cylinder and the L-shaped scatterer. The Daubechies wavelets with $p = 8$ vanishing moments were used. The element threshold was adjusted to maintain a solution error of $(1 \pm 0.02)\%$.

VII. CONCLUSIONS AND COMPARISON WITH OTHER METHODS

Based on the above analysis and observations, we draw the following conclusions about the use of wavelets for solution of electromagnetic integral equations.

First, the use of classical wavelets (such as the Daubechies wavelets) does not appear to reduce the computational complexity of solving the scattering integral equation, but it will reduce solution time by a constant factor. For large problems with smooth surfaces that have only a few isolated corners or sharp bends, and for a fixed solution accuracy, the wavelet-domain impedance matrix will have $\sim \beta N^2$ nonzero elements where β is a very weak function of problem size. The value of β will depend on the desired solution accuracy. For a relative residual error of $\sim 1\%$, we found β to be in the neighborhood of 10%. The cost of converting the impedance matrix to the wavelet basis, using the fast wavelet transform, is $O(N^2)$ and was found to be comparable to the original matrix fill time. The cost of a matrix-vector multiply using the wavelet-domain sparse impedance matrix is reduced by a factor of β compared to the original dense matrix. Thus, the cost of a conjugate-gradient or other iterative solution of the matrix equation is reduced by a factor of β .

Second, the sparsity produced by using wavelet basis functions is seen to be primarily due to the evanescent nature of the fields radiated by the finest resolution (highest spatial frequency) wavelets. The wavelets with broader support and lower spatial frequency have strong interactions with one another. These low-frequency interactions lead to the $O(N^2)$ significant elements in the wavelet-domain impedance matrix.

In contrast, the impedance matrix localization (IML) Method of Canning [11] uses a type of windowed Fourier transform to construct basis functions which radiate in highly directional beams thus reducing the significant interactions in the impedance matrix. This method should also have roughly the same effect as the wavelet transform on the evanescent portion of the current spectrum. By carefully organizing the radiating portion of the current spectrum, this method lowers the computational complexity of the scattering problem. The resulting transformed impedance matrix is reported to have only $O(N)$ significant elements.

Another method which is worth mentioning in this context is the fast multipole method (FMM) of Rokhlin [12]-[15].

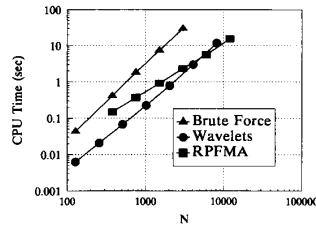


Fig. 14. CPU time required for a matrix-vector multiply as a function of problem size N for E_z polarized scattering from a circular cylinder. The discretization density is 10 points per wavelength.

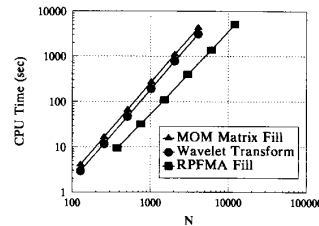


Fig. 15. CPU time required to generate the MoM matrix as a function of problem size N . The wavelet domain impedance matrix was created in two steps: a standard pulse basis MoM matrix fill, followed by a fast wavelet transform.

This method reduces the cost of a matrix-vector multiply for the scattering problem to $O(N^{4/3})$ [15]. As noted in [11], the FMM has the advantage that its effectiveness does not depend on the smoothness of the scatterer surface. This is in contrast with the IML or wavelets, both of which become ineffective for highly irregular surfaces, because they depend on the radiation characteristics of their respective basis functions. Thus, the IML or wavelets would be poorly suited for rough surface scattering problems.

A detailed comparison between wavelets and the FMM is given in Figs. 14–16 for the problem of E_z polarized scattering from a circular cylinder. The FMM results were generated using the ray propagation fast multipole algorithm (RPFMA) reported in [15]. This technique reduces the cost of a matrix-vector multiply to $O(N^{4/3})$. As in the previous results, the discretization density was held fixed at 10 points per wavelength, and a relative residual error of $\sim 1\%$ was maintained for both solution methods. The Daubechies wavelets with $p = 8$ vanishing moments were used. Both methods were used in conjunction with the same conjugate-gradient solver, and all computation was performed on a SUN-SPARC-10 workstation with 128 MB RAM. Single precision arithmetic was used throughout.

Fig. 14 shows the time required for a single matrix-vector multiply. Both wavelets and the RPFMA have a significantly reduced computation time compared to a brute force multiplication using the original, dense, pulse basis MoM matrix. The difference in computational complexity is clearly visible here. The wavelet result grows at the same rate ($O(N^2)$) as the brute force multiply, while the RPFMA has a smaller slope ($O(N^{4/3})$). The wavelet based multiplication has a small enough leading constant, however, that the wavelet

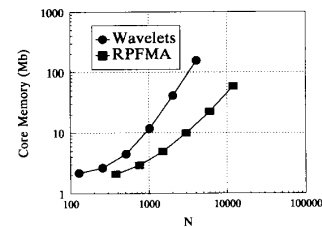


Fig. 16. Core memory required to solve the scattering problem as a function of problem size N . The discretization density is 10 points per wavelength.

domain multiply is faster than the RPFMA multiply when the number of unknowns is less than (roughly) 5000. For more complicated geometries such as the L-shaped scatterer, the cost of the wavelet based multiply would increase somewhat due to reduced sparsity, while the RPFMA would be unaffected as mentioned above.

Another important consideration is the time required to generate the MoM matrix. Fig. 15 shows the time required to fill the original pulse basis MoM matrix and the time required to transform this matrix to the wavelet basis using the fast wavelet transform. As stated earlier, these two times are comparable (for the Daubechies wavelets with $p = 8$ vanishing moments). Also shown is the time required to generate the RPFMA representation of the MoM matrix. The RPFMA fill time is significantly smaller than the wavelet fill time.

It should be noted that all these filling operations need only be carried out once before calling the iterative linear equation solver. When solving the equations for a single right-hand side, the fill time dominates the total solution time. If one wished to solve for many different excitations, however, then the cost of matrix-vector multiplications in the iterative solver would dominate. Thus, depending on the desired results and the problem size, either wavelets or the RPFMA may be more efficient. For problems with $N > 5000$ unknowns, the RPFMA will always be faster.

There are some subtleties in the fill-time results shown here which require further discussion. First, we note that the RPFMA fill time may be further reduced by using the fast Fourier transform or (for very large problems) far-field approximations in the matrix filling calculations. For asymptotically large problems, the fill time complexity reduces to $O(N^{4/3})$ [15]. Also, it is possible to generate the wavelet-basis matrix elements by direct integration in the standard moment method fashion. If one can predict in advance the sparsity structure of the wavelet-domain impedance matrix, it may be possible to significantly reduce the fill time for the wavelet method by computing only the significant wavelet-domain matrix elements. As illustrated by the L-shaped scatterer, however, it may be difficult to predict the sparsity structure for complex scatterer shapes.

Finally, the core memory required by each solution technique is shown in Fig. 16. For wavelets, the core memory grows asymptotically as $O(N^2)$ and is always greater than the memory required for the RPFMA which grows at the slower rate of $O(N^{4/3})$. Again, as for the fill-time requirements, it may be possible to reduce the wavelet memory requirements

by changing the way the wavelet-domain matrix is generated. In our current code, the entire pulse-basis MoM matrix must be generated and stored in core memory, so its fast wavelet transform may be computed efficiently. Thus, storage space is required for both the full pulse basis MoM matrix (N^2 entries) and the sparse wavelet basis matrix (βN^2 entries). It is possible to avoid generating the pulse basis matrix first by directly computing the elements of the wavelet basis matrix. Unless the sparsity structure of the wavelet-domain matrix is known in advance, however, this may require more CPU time, because this approach does not take advantage of the fast wavelet transform algorithm. In any case, the wavelet algorithm would still require storage of βN^2 sparse matrix entries.

In summary, the above described use of classical wavelet basis functions for the solution of electromagnetic integral equations, while reducing solution time by a constant factor, does not appear to reduce the computational complexity of solving the problem. At the same time, we have found it very interesting to study wavelets for electromagnetic applications, and we hope that the discussion here may offer some insights into their use and aid in the future development of fast solution algorithms.

REFERENCES

- [1] H. Kim and H. Ling, "On the application of fast wavelet transform to the integral-equation solution of electromagnetic scattering problems," *Micro. Opt. Tech. Lett.*, vol. 6, no. 3, pp. 168-173, Mar. 1993.
- [2] B. Z. Steinberg and Y. Leviatan, "On the use of wavelet expansions in the method of moments," *IEEE Trans. Antennas Propagat.*, vol. 41, no. 5, pp. 610-619, May 1993.
- [3] D.-S. Wang and G. Welland, "Modeling of electromagnetic scattering using wavelet techniques for geometry modeling and expansion functions," *1993 URSI Radio Sci. Meet. Dig.*, Ann Arbor, MI, p. 277, June 1992.
- [4] R. L. Wagner, G. P. Otto, and W. C. Chew, "Fast waveguide mode computation using wavelet-like basis functions," *IEEE Micro. Guid. Wave Lett.*, vol. 3, no. 7, pp. 208-210, July 1993.
- [5] G. Beylkin, R. Coifman, and V. Rokhlin, "Fast wavelet transforms and numerical algorithms I," *Comm. Pure Appl. Math.*, vol. 44, pp. 141-183, 1991.
- [6] B. Alpert, G. Beylkin, R. Coifman, and V. Rokhlin, "Wavelet-like bases for the fast solution of second-kind integral equations," *SIAM J. Sci. Comput.*, vol. 14, no. 1, pp. 159-184, Jan. 1993.
- [7] G. Strang, "Wavelets and dilation equations: A brief introduction," *SIAM Rev.*, vol. 31, no. 4, pp. 614-627, Dec. 1989.
- [8] I. Daubechies, "Orthonormal bases of compactly supported wavelets," *Comm. Pure Appl. Math.*, vol. 41, pp. 909-996, 1988.
- [9] W. H. Press, S. A. Teukolsky, W. T. Vetterling, and B. P. Flannery, *Numerical Recipes in FORTRAN: The Art of Scientific Computing*, 2nd ed. New York: Cambridge Univ. Press, 1992.
- [10] W. C. Chew, *Waves and Fields in Inhomogeneous Media*. New York: Van Nostrand Reinhold, 1990.
- [11] F. X. Canning, "Improved impedance matrix localization method," *IEEE Trans. Antennas Propagat.*, vol. 41, no. 5, pp. 659-667, May 1993.
- [12] V. Rokhlin, "Rapid solution of integral equations of scattering theory in two dimensions," *J. Comput. Phys.*, vol. 36, no. 2, pp. 414-439, Feb. 1990.
- [13] N. Engheta, W. D. Murphy, V. Rokhlin, and M. S. Vassiliou, "The fast multipole method (FMM) for electromagnetic scattering problems," *IEEE Trans. Antennas Propagat.*, vol. 40, no. 6, pp. 634-641, June 1992.
- [14] C. C. Lu and W. C. Chew, "Fast algorithm for solving hybrid integral equations," *IEE Proc.-H*, vol. 140, no. 6, pp. 455-460, Dec. 1993.
- [15] R. L. Wagner and W. C. Chew, "A ray-propagation fast multipole algorithm," *Micro. Opt. Tech. Lett.*, vol. 7, no. 10, pp. 435-438, July 1994.

Robert L. Wagner was born in Ann Arbor, MI, on October 29, 1965. He received the B.S. degree from Michigan State University, East Lansing, in 1989, and the M.S. degree from the University of Illinois at Urbana-Champaign in 1991, both in electrical engineering.

Currently, he is pursuing the Ph.D. degree at the University of Illinois, where he has worked as a Research and Teaching Assistant. His research interests include wave propagation and scattering, numerical techniques in electromagnetics, inverse scattering, and remote sensing. During the summers of 1991-1993, he was an intern at Schlumberger-Doll Research in Ridgefield, CT, working on electromagnetic problems for geophysical remote sensing applications.

Mr. Wagner received first place in the 1994 IEEE AP-S International Symposium Student Paper Contest. He is a member of Tau Beta Pi.

Weng Cho Chew (S'79-M'80-SM'86-F'93) was born on June 9, 1953, in Malaysia. He received the B.S. degree in 1976, both the M.S. and Engineer's degrees in 1978, and the Ph.D. degree in 1980, from the Massachusetts Institute of Technology, Cambridge, all in electrical engineering.

His recent research interests have been in the area of wave propagation, scattering, inverse scattering, and fast algorithms related to scattering, inhomogeneous media for geophysical subsurface sensing, and nondestructive testing applications. From 1981-1985, he was with Schlumberger-Doll Research in Ridgefield, Connecticut. While he was there, he was a Program Leader and later a Department Manager. From 1985-1990, he was an Associate Professor with the University of Illinois. He is currently a Professor there and teaches graduate courses as well as supervises a graduate research program. His name is often listed in the List of Excellent Instructors on campus. He has authored one book *Waves and Fields in Inhomogeneous Media*, published over 140 scientific journal articles, and presented over 130 conference papers.

Dr. Chew is a member of Eta Kappa Nu, Tau Beta Pi, URSI Commissions B and F, and an active member with the Society of Exploration Geophysics. He is an IEEE Fellow and was an NSF Presidential Young Investigator for 1986. He was also an AdCom member and is presently an associate editor of the TRANSACTION OF THE IEEE GEOSCIENCE AND REMOTE SENSING SOCIETY. He was also an associate editor with the *International Journal of Imaging Systems and Technology*, and has been a Guest Editor of *Radio Science and the International Journal of Imaging Systems and Technology*. From 1989-1993, he was the associate director of the Advanced Construction Technology Center at the University of Illinois.